JCTC Journal of Chemical Theory and Computation

Mechanism of Ultrafast Photodecay in Restricted Motions in Protonated Schiff Bases: The Pentadieniminium Cation

Jaroslaw J. Szymczak,* Mario Barbatti, and Hans Lischka*

Institute for Theoretical Chemistry, University of Vienna, Waehringerstrasse 17, A-1090 Vienna, Austria

Received May 6, 2008

Abstract: Ab initio surface-hopping dynamics simulations for the *trans*-penta-3,5-dieniminium cation (PSB3) are presented imposing different sets of mechanical restrictions in order to investigate the response of the molecular system to certain environmental degrees of hindrance. A general scheme for classification of photoisomerization mechanisms in conjugated chains based on the analysis of torsional angles is proposed allowing direct characterization of the different isomerization mechanisms proposed previously. On the basis of a statistical analysis of 300 trajectories a new photoisomerization mechanism—the Folding Table—was found. This mechanism and the One-Bond-Flip are almost entirely responsible for the photoisomerization process in PSB3.

1. Introduction

Protonated Schiff bases $CH_2(CH)_{n+1}NH_2^+$ (PSBn) constitute a very interesting and important class of molecular systems since they serve as models for studying the photoisomerization of retinal, which is involved in the primary process of vision and represents the driving force for a proton pump through cell membranes of *Halobacterium salinarium*.[1,2] The former process is initiated by a *cis-trans* photoisomerization of 11-*cis* retinal, the chromophore of rhodopsin.[3–7] A related photochemical reaction starts with UV excitation of all-*trans* retinal followed *trans-cis* photoisomerization to 13-*cis* retinal in bacteriorhodopsin.[8,9] These photoisomerization processes belong to the fastest photochemical reactions in nature[3] and have been studied extensively in experimental[1,10–19] and theoretical investigations.[20–27] Extensive quantum chemical calculations have been performed for the computation of photochemical reaction pathways starting from the Franck–Condon region and leading to the conical intersections where ultrafast, radiationless decay to the electronic ground state occurs.[21,28–31] Dynamics calculations[22–27,32,33] have given detailed insights into the actual course of these processes beyond the static analysis. Whereas most of these investigations have been performed for the isolated PSB system, several theoretical investigations have been carried out also with the inclusion of environmental effects.[30,34–41] Extensive calculations with realistic representation of the protein environment have been undertaken for the electronic ground state of rhodopsin[41] and bacteriorhodopsin[42] models including dynamics simulations using quantum chemical and force field methods. Dynamical simulations of the photoisomerization process considering environmental effects are even more challenging due to increased difficulties in performing the excited-state calculations. Combined quantum mechanical/molecular mechanics (QM/MM) approaches have been used for that purpose.[24,43] Because of the excessive computational cost of these simulations only a few trajectory runs could be performed limiting the statistical significance of the obtained results.

Most of the aforementioned theoretical investigations have led to the general picture that the photoisomerization proceeds in a relatively straightforward way by starting with in-plane skeletal relaxation followed by torsion around CC bonds holding double bond character in the ground state. An exception is the recent work of Send and Sundholm[21] based on single-reference time-dependent density functional (TD-DFT) and resolution-of-the-identity coupled cluster to second order (RI-CC2) methods giving a somewhat different picture. In spite of the interesting conclusions drawn in this

* Corresponding author e-mail: jaroslaw.szymczak@univie.ac.at (J.J.S.) and hans.lischka@univie.ac.at.

10.1021/ct800148n CCC: $40.75
Published on Web 07/26/2008

work the reliability of these methods is questionable as comparison of analogous results for smaller PSB chains with multireference approaches show.[25,37,44] In any case, it is clear that, when retinal or a retinal model is considered within the protein pocket, spatial requirements for the *cis-trans* isomerization become essential for the description of the isomerization.

In the present work we want to follow a simpler concept for inclusion of external effects on a PSB chain as compared to detailed QM/MM simulations. Extended dynamics simulations have been performed by mechanically restricting the motion of specific PSB sites by attributing artificially large nuclear masses to terminal hydrogen atoms (for details see below) in a similar way as implemented by Warshel.[27] This technique of mass restrictions has also been successfully used by us for aminopyrimidine[26,45,46] in order to simulate the adenine photodynamics. The advantage of this approach is that the restricted dynamics can be performed at the same computational cost as the nonrestricted approach and allows more freedom in the selection of quantum chemical methods in the dynamics and the calculation of statistically relevant sets of trajectories. These mass restrictions can be viewed as models for the link of retinal to the protein surroundings by the Schiff base bond and for cutting of the retinal end containing the β-ionone ring. One can also look at these restrictions in a more general way as certain general restraints on an unsaturated carbon chain.

Several mechanisms for restricted *cis-trans* isomerizations have been proposed in the literature so far. The simplest one, the torsion around one formal double-bond (one-bond-flip - OBF),[10,30,47] which is supposed to take place primarily in the nonrestricted isomerization, has been put aside because of excessive space requirements. The first alternative, proposed by Warshel based on mixed quantum-classical dynamics simulations,[27] is the bicycle-pedal motion (BP), which consists of the simultaneous torsion of two formal double bonds separated by a single bond. Later on, Warshel and Barboy[48] noted that the isomerization could also take place through a mechanism similar to the BP but with one of the formal double bonds performing only a partial torsional motion. We refer to this mechanism as the nonrigid BP (NRBP). Recently, Frutos et al.[24] have brought new evidence in favor of the NRBP mechanism by their dynamics simulations on retinal. In their investigation, however, only one single trajectory was computed, and it is not possible to draw statistical inferences. Liu and Asato[49] proposed another mechanism named concerted torsion or hula-twist (HT), which consists of the simultaneous torsion of two adjacent bonds followed by skeletal relaxation. The HT mechanism has been extensively discussed in the work of Ruiz et al.[50] and Norton and Houk.[51] Additionally, a new mechanism has been identified in the course of the present dynamics simulations and will be introduced in the current work. The so-called folding-table mechanism (FT) is a combination of three concerted torsions, which will be discussed in detail below.

Although several attempts have been made to verify by means of dynamics simulations[22,23,26,27,34,52,53] how the photoisomerization actually takes place, the somewhat loose definition of the different mechanisms makes the comparison of different data sets difficult. The situation is particularly critical because the freedom of motion in the dynamics simulation usually produces geometries that are far from ideal prototypes. Our present goal is to utilize the PSB3 system, considered as the simplest example in retinal modeling,[28,54,55] to establish clear definitions of these mechanisms, which can be directly applied to the classification of the dynamical processes occurring in molecular chains such as PSBn. Application of this classification scheme is not restricted to PSB3 chains but can in principle be used for any molecular chain presenting *cis-trans* isomerization.

2. Computational Details

The quantum chemical calculations were performed at the complete active space self-consistent field (CASSCF) and multireference configuration interaction (MRCI) levels. The CASSCF calculations were carried out using a CAS(6,6) averaging over the two lowest singlet states (denoted as SA-2-CASSCF(6,6)). The reference space for the MRCI calculations is based on the SA-2-CASSCF(6,6) calculation. For the MRCI calculations a CAS(4,5) reference space was chosen (denoted as MRCI(4,5)). This selection was chosen on the basis of a natural orbital occupation criterion moving the lowest CASSCF orbital (occupation 1.96) into the doubly occupied space. The CI expansion included either all single and double substitutions (MR-CISD) or only single excitations (MR-CIS) from the reference space. When double excitations are included, the generalized interacting space restriction[56] was adopted. The 3−21G and 6−31G* basis sets were used.[57,58]

On-the-fly ab initio nonadiabatic dynamics calculations were performed using Tully's surface hopping approach.[59,60] The nuclear motion is computed by solving Newton's equations based on the Born−Oppenheimer potential obtained by the respective quantum chemical method. The integration of the classical equations is performed by means of the velocity-Verlet algorithm[61] in time-steps of 0.5 fs. The total simulation time was 200 fs. The time-dependent wave function is expanded in the adiabatic representation, and the time-dependent electronic Schrödinger equation is integrated using the fifth-order Butcher algorithm.[62] In order to further improve the numerical integration of the time-dependent Schrödinger equation, a smaller time step $\Delta t' = \Delta t/m_s$ ($m_s = 20$) is used, with the relevant quantities interpolated from t to $t + \Delta t$. The obtained time-dependent adiabatic populations were corrected for decoherence effects[63] ($\alpha = 0.1$ hartree) and used for computing the surface hopping probabilities of a nonadiabatic transition according to the fewest-switches algorithms proposed by Tully[59,60] and Hammes-Schiffer and Tully.[64] At each time-step, a random event is used to decide whether the system will switch to another state. The momentum after frustrated hoppings was kept constant, and after actual hoppings it was readjusted along the nonadiabatic coupling vector. The initial conditions for the simulated trajectories are generated by means of a ground-state Wigner distribution by treating the nuclear coordinates and momenta within the quantum-harmonic-oscillator approximation.

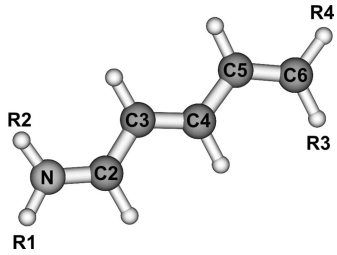

Figure 1. Numbering of atoms in PSB3 with indication of restrictions; nonrestricted PSB3: R(1−4) = H; PSB3 with two restrictions: R1 = R4 = "restricted hydrogen", R2 = R3 = H; PSB3 with 4 restrictions: R(1−4) = "restricted hydrogen".

As already mentioned above, in addition to the nonrestricted dynamics, restricted simulations were performed. The restrictions were imposed by increasing the masses of the terminal hydrogen atoms. Two sets of restrictions were constructed. In the first set, two hydrogen atoms (R1 and R4 in Figure 1, later on denoted as restricted hydrogens) were modified. The restricted hydrogens were positioned in *trans* orientation to each other. This choice is designed to model the situation where the restricted hydrogen atom located at the nitrogen end represents the binding of PSB3 to the protein, whereas the other restricted hydrogen atom stands for the rest of the retinal chain. After preliminary test calculations a mass of 1000 au was used. This choice practically fixes the positions of these hydrogen atoms during the dynamics. In the second set of restrictions, masses of 1000 au were given to all four terminal hydrogens. Using these two sets of restrictions, dynamics simulations starting at the *trans* isomers of PSB3 were performed.

A total of 300 trajectory calculations for the restricted PSB3 systems were performed (100 for each of the system with no, two, and four restrictions). The CASSCF and MRCI calculations have been performed using the COLUMBUS program system[65–67] and the methods for analytic computation of gradient and nonadiabatic coupling vectors.[68–72] The on-the-fly surface-hopping calculations were carried out by means of the program system NEWTON-X[25,73] using the quantum chemical data computed by COLUMBUS at each time step. The automatic classification of the observed motions was performed using an analysis program developed in our group.

3. Validation of the Theoretical Level

In on-the-fly dynamics calculations, energies, gradients, and nonadiabatic coupling vectors have to be computed at each time step leading to hundreds of thousands of individual quantum chemical calculations. Therefore, it is crucial to find a balance between the quality of the approach (choice of method and basis set) and the computational cost. Under these circumstances accuracies as they are achievable in conventional single-point calculations and geometry optimizations are out of reach. Thus, before starting such time-consuming dynamics simulations, static test calculations on the investigated systems were carried out with the aim of judging the performance of different approaches for calculating the excited-state energies and finding the optimal procedure. The main purpose of this part of the investigation is the assessment of the unpolarized 3−21G basis for use in the main body of dynamics calculations. This basis set, which has been examined and used in recent dynamics investigations of other groups[74–76] and in our group as well,[25] is a natural candidate for achieving substantial savings in computer time if the resulting energy surfaces are not distorted too much. However, it is also clear that with the drastic reduction in basis set size certain inadequacies are unavoidable. Additionally, the influence of the choice of the quantum chemical method has been investigated as well.[37] This assessment is performed in several steps. In step 1 the critical points on the energy surfaces relevant for the photoisomerization process−vertical excitation energies, the S_1 energy minimum (S_1min) under planarity restriction, and the structure for the minimum on the crossing seam (MXS) of the torsion around the central bond−were investigated. In step 2 approximate reaction paths starting from S_1min to the S_0/S_1 MXS have been examined. The reaction paths have been obtained by means of the method of linear interpolation of internal coordinates (LIIC) between these two structures using natural internal coordinates as defined by Fogarasi et al.[77] Finally, the lifetimes of dynamics calculations are compared with previous results.[23,24,26,27,33–35]

Figure 2a shows the differences in bond lengths along the *trans*-PSB3 chain for the S_1min structure employing the SA-2-CASSCF(6,6), MR-CIS(4,5), and MR-CISD(4,5) methods and the 6−31G* and 3−21G basis sets. Full Cartesian coordinates are given in the Supporting Information. Results for the optimized S_1min structures obtained with the smaller basis sets agree quite well with those obtained with the 6−31G* basis. Differences in bond distances are mostly smaller than 0.01 Å within the same method. The largest difference of 0.04 Å was observed for the C3−C4 bond with MR-CISD(4,5). However, all methods predict this bond to be the longest one, and, therefore, the torsion around it is expected to be favored. The second largest difference between both basis sets is the elongation of the N1−C2 bond by ∼0.015 Å for the CASSCF/3−21G calculation. This difference is also reflected in dynamics calculations for CASSCF/3−21G where a secondary channel of deactivation due to the torsion around the N1−C2 bond has been observed.[25] The use of the MR-CIS/3−21G method removed this artifact due to a reduction of the N1−C2 bond in comparison to CASSCF. The basis set differences in bond lengths observed for the MXS structure are of the same order as in the case of the S_1min structures (Figure 2b and the Supporting Information for Cartesian coordinates). In agreement with previous investigations[31,53–55] the geometry of the MXS is reached by a ninety degrees rotation around the central double bond and concomitant adjustment of bond lengths.

Figure 3a shows that the shapes of the LIIC curves are very well reproduced by the calculations employing the smaller basis set. Differences are observed primarily in the neighborhood of the S_1min structures and amount to about 0.3 eV in the maximum and result from differences in the quantum chemical method rather and not from the basis set. Furthermore, the energies of the aforementioned key points of the photoisomerization process relative to the ground-

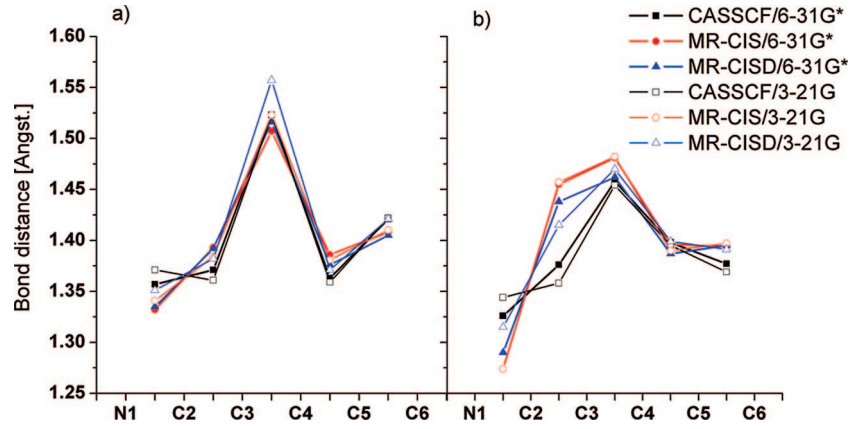

Figure 2. CN and CC bond lengths for unrestricted PSB3 in a) S_1 minimum and b) for the S_1/S_0 MXS determined for different approaches employing the 6−31G* and 3−21G basis sets.

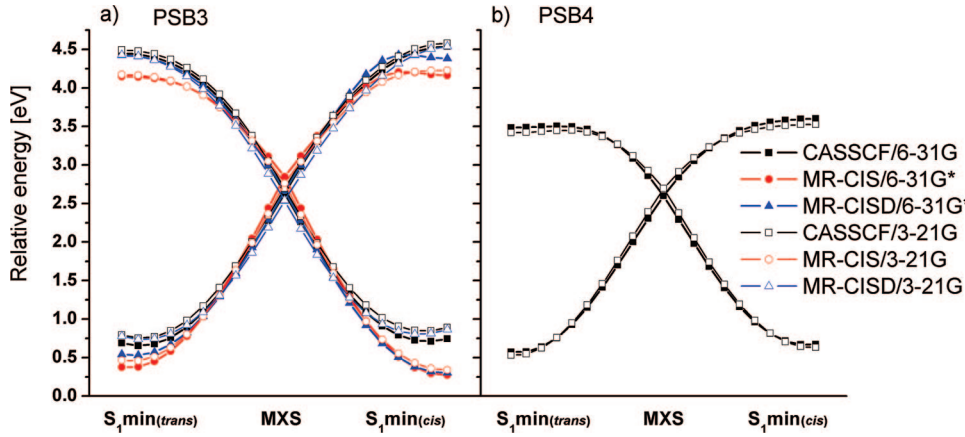

Figure 3. Energy paths connecting the minimum in the S_1 state (*trans* isomer) to the MXS and the MXS to the minimum in the S_1 state (*cis* isomer). a) PSB3 calculated at the (SA-2) CASSCF(6,6), MR-CIS(4,5)/CASSCF(6,6) and MR-CISD(4,5)/CASSCF(6,6) levels using the 6−31G* and 3−21G basis sets and b) PSB4 calculated at the SA-2-CASSCF(8,8) level using the 6−31G* and 3−21G basis sets. Energies are given relative to the optimized ground-state structure.

state minimum are quite the same for different basis sets (see Table 1). Typical differences are close to 0.1 eV or less for the CASSCF and MR-CIS methods. Slightly larger differences reflecting the corresponding changes in geometry for the same level are observed only for the MR-CISD method.

Moreover, the lifetime of PSB3 obtained in the current work is not significantly affected by the choice of the two examined basis sets. The average lifetime of 96 fs obtained from the trajectories with no restrictions and the 3−21G basis agree well with the results obtained with the 6−31G* basis set (98 fs for unrestricted dynamics).[26]

To verify our choice of computational method and basis set even further, especially in view of future applications to larger protonated Schiff bases, calculations on the 5-*cis* and 5-*trans* isomers of the hepta-3,5,7-trieniminium cation (PSB4) were performed as well. Similar to PSB3 a very good performance of the 3−21G basis set was observed. In the Supporting Information (Table SI1) vertical excitation energies and energies of key points for both isomers of PSB4 are collected. The calculations employing the CASSCF(8,8)/6−31G* and CASSCF(8,8)/3−21G methods show very good agreement. This is further assured by LIIC potential curves (Figure 3b) computed for both levels of theory.

Combining the all just-described experience, the MR-CIS/3−21G approach was chosen for performing the dynamics calculations of PSB3. Tests using the MR-CISD/3−21G approach did not show significant improvement, and the cost of such calculations is severe making it extremely difficult to obtain statistically significant samples. The present systematic survey gives us the confidence that the major features of the dynamics such as the structural and energetic changes and lifetimes are reasonably well reproduced. We expect—and test calculations on PSB4 presented here confirm this expectation—that the performance of the 3−21G basis will be of similar good quality also for the larger PSB members. However, it is also clear that great care has to be exercised when trying to extend this experience to other molecular systems.

4. Classification Scheme

The purpose of this subsection is to describe the methods used in this work to analyze the geometrical evolution of the PSB3 chain. The behavior of the dynamics of PSBn systems during the photodecay has been characterized in previous theoretical investigations as a two-step process in terms of initial skeletal stretching and subsequent torsional

Table 1. Relative Vertical Excitation Energies (VEE), Energies of S_1min, and MXS for *cis* and *trans* Isomers of PSB3

	CASSCF	MR-CIS	MR-CISD
	PSB3 (*trans*)		
S_0[a]			
6−31G*	−248.250193[b]	−248.349618[b]	−248.891836[b]
3−21G	−246.875623[b]	−246.959738[b]	−247.331737[b]
VEE			
6−31G*	4.84	4.39	4.61
3−21G	4.93	4.45	4.70
E(S_1min)			
6−31G*	4.45	4.15	4.42
3−21G	4.49	4.17	4.43
E(MXS)			
6−31G*	2.63	2.85	2.66
3−21G	2.70	2.76	2.53
	PSB3 (*cis*)		
S_0[a]			
6−31G*	0.15	0.16	0.14
3−21G	0.13	0.15	0.12
VEE			
6−31G*	4.68	4.22	4.45
3−21G	4.81	4.31	4.57
E(S_1min)			
6−31G*	4.54	4.16	4.38
3−21G	4.58	4.22	4.54

[a] Geometries obtained at the B3LYP/SV(P) level of theory. [b] Values in Hartrees.

motion around a double bond.[54,78,79] In the initial stage of the dynamics the system relaxes by adjusting the bonds length, elongating the double bonds, and shortening the single bonds.[54,78–80] After adjusting all bonds, the molecular system proceeds to the second step of the dynamics. The crossing seam is reached by skeletal torsions around one[54] or more bonds.[24,27,48] When the system then switches from the excited state to the ground state along a torsional mode, it can either continue or reverse the motion that led to the MXS and further relax to the final product geometry.

The initial phase of the quasi-planar CC bond length relaxation is relatively short[24,26,33] (10−15 fs) and seems to be straightforward, whereas the second phase of torsional modes is certainly much more involved and finally determines the outcome of the dynamics. Therefore, we concentrate in our analysis on the torsional phase. In order to get better insight into this process this step was analyzed by dividing it into two stages. The first stage concerns the torsions leading to the conical intersection, and the second stage relates to the continuation of the motion on the ground-state energy. Both stages are characterized by complicated torsional modes coupled to bending and stretching modes. To characterize the evolution of the torsional angles in the first stage differences $\Delta\theta_i = \theta_i^{hop} - \theta_i^0$ are computed for all skeletal torsional angles where θ_i^0 is taken from the ground-state geometry as given by the initial conditions of the trajectory and θ_i^{hop} is the angle at the time of the hopping. The dihedral angles used in the analysis are θ_1 = R1−N−C2−C3, θ_2 = N−C2−C3−C4, θ_3 = C2−C3−C4−C5, θ_4 = C3−C4−C5−C6, and θ_5 = C4−C5−C6−R4 (for numbering see Figure 1). Analysis of these angles in the course of the dynamics will lead to wide distributions. For examples see Figures 4 and 5, which are discussed below. From these distributions no obvious separation in different classes can

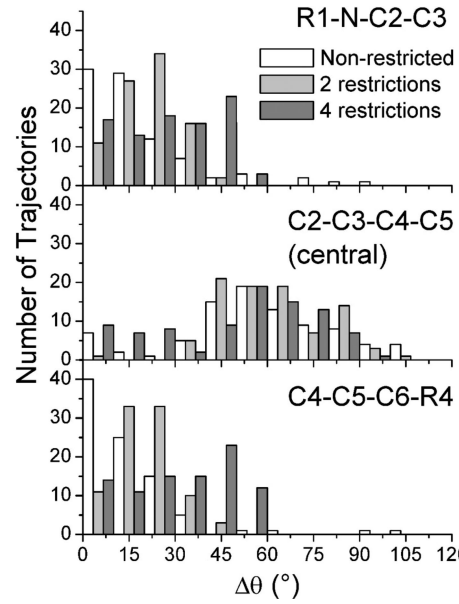

Figure 4. Histograms of changes in torsional angles of the formal double bonds ($\Delta\theta_i$, i = 1,3,5) at the moment of hopping relative to the planar ground-state structure.

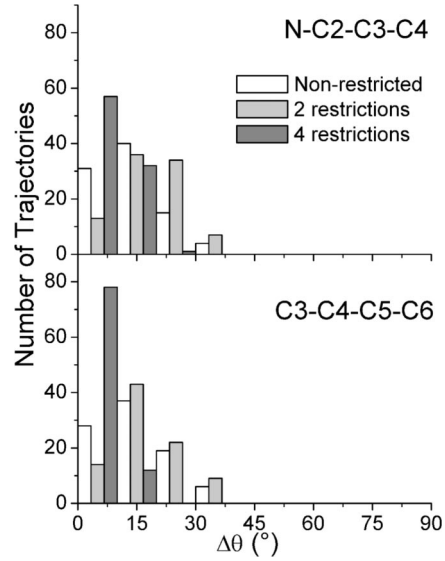

Figure 5. Histograms of changes in torsional angles of the formal single bonds ($\Delta\theta_i$, i = 2,4) at the moment of hopping relative to the planar ground-state structure.

be observed. In order to achieve a simple classification, $\Delta\theta_i$ values have been assigned to one of three groups in 30° ranges between 0 and 90°. These groups have been labeled according to their progress in the torsional mode as discussed below. Test calculations using different angle increments have shown that this division represents a good compromise between sufficiently fine granularity for the description of individual classes of structures and simplicity in terms of number of classes.

The purpose of this classification is to give a rough overview of an otherwise complicated and detailed situation. In spite of the admittedly arbitrariness of this procedure with respect to the selected angle thresholds we think that it is useful and allows for simple classification schemes. If the change in a given torsional angle was located between 0°

Table 2. Examples of $\{\Delta\theta\}$ Patterns Used in the Classification of the Types of Motions in PSB3[a]

	dihedral angle change $\Delta\theta_i$				
	N−C2	C2−C3	C3−C4	C4−C5	C5−C6
OBF	a	a	c	a	a
BP	a	c	a	c	a
NRBP	a	c	a	b	a
HT	a	a	c	c	a
FT	b	a	c	a	b

[a] For OBF, for example, only the pattern corresponding to the central torsion is shown. a - $0° \le \Delta\theta_i < 30°$. b - $30° \le \Delta\theta_i < 60°$. c - $60° \le \Delta\theta_i \le 90°$.

and 30°, this change has been considered as "not relevant" for the *trans-cis* isomerization and has been labeled as "*unchanged*" (denoted by the letter 'a'). When a given $\Delta\theta_i$ was situated in the interval between 30° and 60°, the change was classified as "*partial*" (denoted 'b'). The third group consisted of angles that had changed by more than 60°. This change was considered as "*significant*" (denoted 'c').

Using this criterion, any given PSB3 geometry can be classified according to its five dihedral changes $\Delta\theta_i$ or $\{\Delta\theta_i\}$ patterns, and the progress in the torsional modes can be analyzed quickly. Table 2 shows examples of $\{\Delta\theta\}$ patterns observed in the dynamics runs corresponding to each of the five types of isomerization mechanisms mentioned in the Introduction. The one-bond-flip (OBF)[10,30,47] is defined here as the process for which only one *significant* or *partial* change in a dihedral angle is found, whereas all other dihedral angles remain *unchanged*. The folding-table (FT) mechanism can be described as a combination of three torsions, with the main central torsion accompanied by two *partial* torsions on both sides separated by one *unchanged* dihedral angle each. The bicycle-pedal (BP)[27] mechanism is characterized by simultaneous *significant* changes of two dihedrals that are separated by one dihedral angle in between that stays *unchanged* during the motion. The nonrigid bicycle-pedal (NRBP) mechanism[48] represents a case similar to BP; however, the torsion around one of the bonds proceeds slower or starts later than the other. This behavior results in a *partial* change of the corresponding dihedral angle, which resembles a situation when one of the "pedals" is loose and the motion is no longer rigid. The last mechanism, the hula-twist[49–51] (HT) is described as a simultaneous *significant* change of two neighboring dihedral angles not accompanied by any other torsion.

The second stage of the torsional part of the dynamics—the behavior of the molecule after hopping to the ground state—has been examined from two points of view. The first one concerns the continuation of the motion leading to the conical intersection, and the second one its outcome in terms of the final product. For this purpose the following scheme was applied. The torsional motion of PSB3 is checked 20 fs after the hopping for changes in the dihedral angles with respect to the value at the hopping. Only torsional angles characteristic for the given type of motion are investigated. In the OBF case, for example, only the dihedral angle with *significant* or *partial* change is checked. If this change is larger than a threshold of $\delta = 20°$ or smaller than $-\delta$, then the motion is classified as *continued* or *reversed*, respectively. If this threshold is not reached within this time, the motion is examined again after each 5 fs. Previous calculations had shown that major changes of dihedral angles proceeded within a time range of about 50 fs.[24,39,43,52] Therefore we decided to continue this analysis for a somewhat longer time (60 fs after the hopping event), always trying to classify the motion either as *continued* or *reversed*. In addition to checking the motion toward the conical intersection with respect to continuation or reversal, the question is examined whether this motion is so pronounced that it also leads to a *cis* or *trans* structure within 60 fs. For this purpose all five dihedral angles θ_i are examined. The designated fragment is considered as *trans* (E) if the corresponding dihedral angle was in the range of $180° \pm 60°$ or *cis* (Z) if the angle fell into the range of $0° \pm 60°$. The geometry is classified in terms of $\{\theta_i\}$ patterns. The EEEEE and EEZEE patterns, for example, correspond to the all-*trans* and to the 3-*cis* structures, respectively. It is expected that the application of such a final product analysis should be especially important for the classes of restricted systems. Since the size of the PSB3 molecule is relatively small and full relaxation is not allowed in this case, the excess energy can cause additional torsions, usually not observed in the case of the nonrestricted dynamics. Therefore, especially with 4-restricted PSB3 the direct continuation of the motion leading to the conical intersection need not result in creation of the corresponding final product in many cases. Independently, the final structure is determined at the end of the simulation time.

5. Results and Discussion

5.1. Mechanism Leading to the Conical Intersection. The main mechanism leading to the conical intersection in unrestricted PSB3 is the OBF around the central C3−C4 bond.[22,26,30,54] The existence of external restrictions, however, modifies the character of this mechanism by enforcing additional torsions. The analysis of $\Delta\theta_i$ values at the time of hopping (Figures 4 and 5) indicates that the distribution of changes in torsional angles extends significantly beyond 30° only for bonds corresponding to double bonds in the ground state. Thus, practically only those bonds are involved in the initial phase of the isomerization process, while torsion around formal single bonds is of minor importance. As expected, the major changes in the torsional angles are observed for the central CC bond, which shows broad peaks at around 60° for all types of dynamics simulations, unrestricted, 2- and 4-fold restricted (Figure 4). This fact correlates well with the strong elongation of this bond in the planar S_1 minimum structure displayed in Figure 1. The fact that the conical intersection is on the average encountered at torsional angles significantly smaller than the 90° of the MXS has been already observed and discussed previously.[26,29]

All trajectories have been analyzed according to $\{\Delta\theta_i\}$ patterns presented in the Classification Scheme described above. This analysis is summarized in Table 3. In the case of the nonrestricted dynamics and the dynamics with two restrictions, the dominating fraction of trajectories follows the OBF to the conical intersection. In the nonrestricted case,

Table 3. Statistics of the Motions for all-*trans* PSB3 Leading to the Conical Intersection (in % of Trajectories)

system	OBF	FT	other motion	no hopping
no restrictions	91	0	4[a]	5
2 restrictions	75	9	14	2
4 restrictions	33	55	0	12

[a] All 4 trajectories showed $OBF_{(C3=C4)}$ accompanied by neighboring rotation slightly (~1°) larger than 30°.

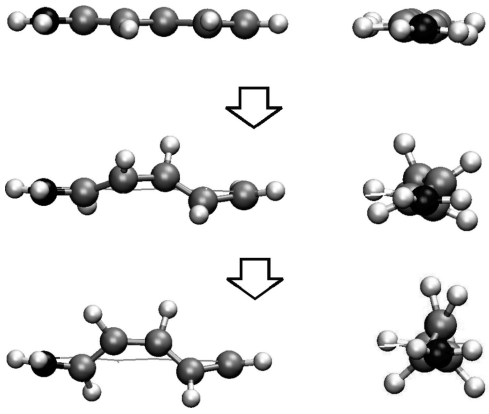

Figure 6. Characterization of the folding-table mechanism (snapshots taken from an actual trajectory). The line given in the second and third snapshot represents the initial chain.

the OBF is realized entirely by torsion around the central bond. Additional analysis of trajectories classified as "other motion" showed that all of them also feature the OBF mechanism, accompanied by *partial* neighboring torsion changes exceeding 30° slightly by ~1°. For the system with two restrictions, 75% of trajectories reach the conical intersection by rotating around the central bond. In both cases no additional isolated rotations at the ends of the PSB3 chain have been observed. Similar to the unrestricted system additional analysis of the "other motion" trajectories represent a situation similar to the one-bond-flip, or alternatively a folding-table process occurs, which is accompanied by a *partial* single bond rotation. This latter torsion angle change is, however, larger (average of 5° beyond 30°) than in the unrestricted dynamics, a fact which precludes them from being classified as an OBF or FT according to our criteria (see also Figures 4 and 5). A minor fraction of trajectories with two restrictions (9%) followed the FT mechanism.

With four restrictions the percentage of OBF drops to 33%. Since all terminal hydrogen atoms are fixed, torsion around the central bond is accompanied by other structural adjustments within the heavy-atom skeleton, while the possibility of the adjustments made by extended motion of the terminal heavy atom is ruled out. As a consequence of these restrictions the FT mechanism, illustrated in Figure 6, becomes dominant. The character of the main torsion resembles an OBF; however, one observes additional *partial* torsions at the terminal bonds on either side of PSB3. These partial torsions lead to a rise of the central CC bond above the original PSB3 plane.

It is worth noting that the other mechanisms that have been suggested to occur in restricted isomerizaton−BP, NRBP, and HT−have not been observed at all during the PSB3 dynamics.

Table 4. Motions after the Hopping (in % of Trajectories Given at the Time of Hopping (See Table *3*))

	OBF		FT		
system	cont.	rev.	cont.	rev.	no classification possible[a]
no restrictions	70	70	0	0	0/0
2 restrictions	65	32	62	38	3/0
4 restrictions	70	27	40	49	3/11

[a] Rrelative to all trajectories assigned to OBF/FT.

Table 5. Fraction of Trajectories (in % of *Continued* Motion Given in Table *4*) after the Hopping Leading to 3-*cis* or 3-*trans* PSB3 (See Text for Explanation)

	OBF			FT		
	cont. motion			cont. motion		
system	*cis*	*trans*	undeterm	*cis*	*trans*	undeterm
0R	89	5	6	-	-	-
2R	84	16	0	100	0	0
4R	22	13	65	32	5	63

5.2. Motion after Surface Hopping. The motion after hopping to the ground state is important since it will determine the final product formation. Several situations can be distinguished. The motion leading to the conical intersection is *continued* or *reversed*, or the molecular system stays in the vicinity of the conical intersection at least for the time of the analysis (60 fs, see the section on the Classification Scheme). Since in this work only the isolated PSB3 system is investigated, no energy transfer to the environment can occur, and the dynamics correspond to a vibrationally hot motion in the ground state during this stage. Therefore, additional vibrational modes may be activated by means of internal vibrational relaxation. In the course of the time period (200 fs) that was investigated here, such vibrational activation occurred mostly in the case when the *continued* motion was observed and new torsions around other bonds inactive in the earlier stages of the dynamics became important. On the other hand, the analysis presented below shows that when a *reversed* motion is observed, it reverses always with 100% efficiency.

Table 4 presents the results of the analysis after the hopping with regard to motion continuation or reversal with a maximum assessment time of 60 fs. Further analysis determining whether the examined torsion leads at least temporarily within a 60 fs time span after the hopping to an associated *cis* or *trans* structure is presented in Table 5. In the nonrestricted system 70% of trajectories classified as OBF continued this torsion after hopping (Table 4). The results given in Table 5 show that the majority (89%) of *continued* motion resulted in the formation of *cis*-PSB3. A similar trend was observed for the doubly restricted dynamics, where 65% of OBF motions (Table 4) leading to the conical intersection also led to *cis*-PSB3 with an efficiency of 84% (Table 5). The situation changes when the fully restricted system is regarded. The ratio of the *continued* motions remains approximately the same (70%); however, only 22% of them end up in the *cis* structure. This drop is accompanied by a very large percentage of undetermined geometries (65% of *continued* OBF). This fact is closely related to the restriction imposed on the system, which simply makes the change of

Table 6. Summary of Photoproduct Analysis (in % of All Trajectories) after the Hopping (Table *5*) and at the End of the Dynamics (Values in Parentheses)

product conformation	corresponding motion	*trans* PSB3		
		0R	2R	4R
EEEEE	-	32(21)	44(39)	40 (55)
EEZEE	$OBF_{C3=C4,}$ FT	59(18)	51(46)	12(3)
other		(17)[a]		
not assigned		4(39)	3(13)	36 (30)
no hopping (excluded from analysis)		5	2	12

[a] Other products: EZZZE(2), EEZZE(9), EZEEE(5), EEEZE(1).

the central torsional angle beyond 120° extremely difficult. In this case the central torsion stays in the range between 60° and 120°. On the other hand, when the motion leading to the conical intersection is *reversed* after hopping, reversion proceeds completely in all cases regardless of the type of motion and system. The statistical analysis of the FT motion for the restricted systems resembles that for the OBF: 62% and 40% of the initial motion is *continued* after the hopping for the doubly and fully restricted system, respectively. In the case of the fully restricted system continuation always implies rotation around the central bond since it is almost impossible to perform an extended rotation around a terminal double bond. For the dynamics with two restrictions any other motion beyond that around the central bond was not observed either. Yields of the product formation in the FT case are comparable to that of the OBF (Table 5). However, it is worth mentioning that similar to the OBF motion in more than half of the cases with four restrictions it was not possible to determine the final product of the *continued* motion unambiguously.

As the last step of the analysis the final structure at the end of the dynamics run was determined independently of the analysis of the PSB3 motion in the different stages of the dynamics (see Table 6). It is interesting to note that the differences between the yields of product formation examined after the hopping to the ground state and at the end of the dynamics are substantial, especially for the unrestricted case. They reflect the changes due to the vibrationally hot dynamics in the ground state after the initial product assignment was made. This is also manifested by the large number of structures that could not be assigned to one of the types of torsional motion at the end of the dynamics since at least one of the dihedral angles was located between 60° and 120°, i.e. far away from planarity. Nevertheless, the trends of the product formation are preserved and vary systematically by reducing the amount of 3-*cis* (EEZEE) and increasing the all-*trans* product formation (EEEEE). Although restricted PSB3 in gas phase is certainly a poor model for quantitative comparisons with real processes taking place in bacteriorhodopsin, it is worth noting that the experimental quantum efficiency of the reaction following the photoexcitation is 0.64,[81] which is well comparable with the present results.

5.3. Lifetimes. The depopulation of the S_1 state as a function of time is illustrated in Figure 7. This figure shows the S_1 occupation defined as the fraction of trajectories in the S_1 state in each time step. The occupation remains constant for a certain time t_d after which it starts to decrease in an exponential way from there on.

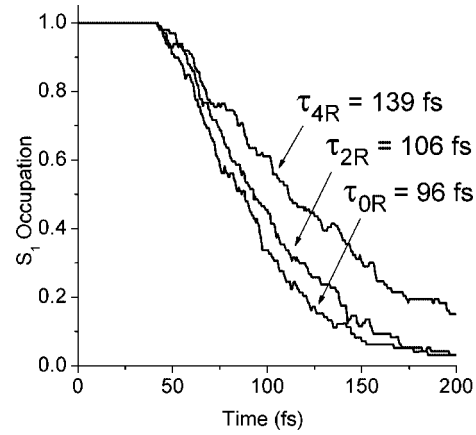

Figure 7. Average occupations of the excited state and lifetimes of trajectories for all studied systems.

The lifetimes $\tau = t_d + t_e$ were obtained by fitting the S_1-state occupation with the function $f(t) = \exp(-(t-t_d)/t_e)$ for all studied systems. The systematic increase of the lifetimes (96, 106, and 139 fs for no, two, and four restrictions, respectively) is consistent with the growing number of restrictions, which makes it increasingly difficult to reach the conical intersection. The change from no to two restrictions has a rather small influence on the lifetime, whereas the change from two to four restrictions is more significant. Currently obtained lifetimes agree well with our recent results[26] and fit well into the range of previous theoretical (80−200 fs)[24,27,33–35] and experimental (100−300 fs)[10,12,14,82,83] findings on Rh and bR and their models.

6. Conclusions

In this work the results of ab initio surface-hopping dynamics simulations for the *trans*-PSB3 cation have been presented using two sets of mechanical restrictions. In the first set the masses of two terminal hydrogen atoms located at opposite ends of the PSB3 chain were kept fixed. In the second set all four terminal hydrogen atoms were restricted. Our main goal has been to analyze and characterize the actual motions occurring in the dynamics of the restricted PSB3 system and compare them to different idealized mechanisms (one-bond-flip (OBF), bicycle-pedal (BP), nonrigid bicycle-pedal (NRBP), hula-twist (HT), and folding-table (FT)).

At the beginning, a survey of important sections of the ground- and excited-state energy surfaces for *cis*- and *trans*-PSB3 and PSB4 including conical intersections has been performed showing that relatively small basis sets can reproduce essential features of these surfaces and the nonadiabatic dynamics on them quite well. This finding reduces the computational cost of the on-the-fly dynamics approach substantially allowing the computation of a relatively large number of trajectories (300 in total) under several conditions. Thus, at least a reliable global picture of the processes occurring in the dynamics of PSB3 system can be given in this way.

The analysis of trajectories shows that for the first stage of the dynamics (the motion leading to the conical intersection) the nonrestricted and doubly restricted cases are dominated by the OBF mechanism. This mechanism, however, decreases in importance with the increase of the number of restricted atoms. In the dynamics with two and four restrictions, a mechanism not previously reported in the literature termed folding-table (FT) was observed. This mechanism is related to the OBF and consists of the torsion around the central bond together with simultaneous partial torsions (about 45°) around the two other formal double bonds. Although the FT mechanism is statistically not important for the doubly restricted case, it dominates in the case of four restrictions. Besides OBF and FT no other of the standard mechanisms were observed. In the doubly restricted system, a substantial number of events (14%) was found that connects the central torsion with a torsion at the neighboring bond by slightly more than 30°.

The second stage of the dynamics—the continuation after hopping to the ground state—gave interesting information on the continuation or reversal of the process leading to the conical intersection and on the possibility of product formation. A major percentage of the trajectories continues the motion which has led to the conical intersection. For no and two restrictions, in a large fraction of cases the motion is even continued up to the formation of the *cis* product for OBF and FT. This drastically changes for the four-restricted case where even the initial continuation of the motion leads only in very few cases to the *cis* product. After having reached a specific structure, the vibrationally hot motion continues, and at the end of the dynamics simulation the originally observed structure was lost again. This happens especially in the unrestricted case. The degree of restriction on the terminal hydrogen atoms has an influence on lifetimes as well. The change from no to two restrictions is rather small, whereas the change from two to four restrictions is more significant.

The application of the classification of torsional motions along a chain of conjugated π-bonds is general and straightforward. They allow easy automation and analysis of dynamics runs without significant human interference and should be applicable to other cases beyond the present application to protonated Schiff bases.

Acknowledgment. This work was supported by the Austrian Science Fund within the framework of the Special Research Program F16 (Advanced Light Sources) and Project P18411-N19. We are grateful for technical support and computer time at the Linux PC cluster Schrödinger III of the computer center of the University of Vienna and Wroclaw Centre for Networking and Supercomputing at Wroclaw University of Technology.

Supporting Information Available: Cartesian coordinates of the optimized geometries (minima and MXS structures) used in this study for all methods applied and vertical excitation energies and energies of key points for both isomers of PSB4. This material is available free of charge via the Internet at http://pubs.acs.org.

References

(1) Wald, G. *Science* **1968**, *162*, 230–&.

(2) Oesterhelt, D.; Stoeckenius, W. *Proc. Natl. Acad. Sci. U.S.A.* **1973**, *70*, 2853–2857.

(3) Birge, R. R. *Biochim. Biophys. Acta* **1990**, *1016*, 293 327.

(4) Palings, I.; Pardoen, J. A.; Vandenberg, E.; Winkel, C.; Lugtenburg, J.; Mathies, R. A. *Biochemistry* **1987**, *26*, 2544–2556.

(5) Birge, R. R. *Annu. Rev. Biophys. Bioeng.* **1981**, *10*, 315–354.

(6) Schoenlein, R. W.; Peteanu, L. A.; Mathies, R. A.; Shank, C. V. *Science* **1991**, *254*, 412–415.

(7) Wang, Q.; Schoenlein, R. W.; Peteanu, L. A.; Mathies, R. A.; Shank, C. V. *Science* **1994**, *266*, 422–424.

(8) Haupts, U.; Tittor, J.; Oesterhelt, D. *Annu. Rev. Biophys. Biomol. Struct.* **1999**, *28*, 367–399.

(9) Neutze, R.; Pebay-Peyroula, E.; Edman, K.; Royant, A.; Navarro, J.; Landau, E. M. *Biochim. Biophys. Acta-Biomembranes* **2002**, *1565*, 144–167.

(10) Kukura, P.; McCamant, D. W.; Yoon, S.; Wandschneider, D. B.; Mathies, R. A. *Science* **2005**, *310*, 1006–1009.

(11) Schenkl, S.; van Mourik, F.; Friedman, N.; Sheves, M.; Schlesinger, R.; Haacke, S.; Chergui, M. *Proc. Natl. Acad. Sci. U.S.A.* **2006**, *103*, 4101–4106.

(12) Kobayashi, T.; Saito, T.; Ohtani, H. *Nature* **2001**, *414*, 531–534.

(13) Kukura, P.; McCamant, D. W.; Mathies, R. A. *Annu. Rev. Phys. Chem.* **2007**, *58*, 461–488.

(14) McCamant, D. W.; Kukura, P.; Mathies, R. A. *J. Phys. Chem. B* **2005**, *109*, 10449–10457.

(15) Terentis, A. C.; Ujj, L.; Abramczyk, H.; Atkinson, G. H. *Chem. Phys.* **2005**, *313*, 51–62.

(16) Atkinson, G. H.; Ujj, L.; Zhou, Y. D. *J. Phys. Chem. A* **2000**, *104*, 4130–4139.

(17) Jager, F.; Ujj, L.; Atkinson, G. H.; Sheves, M.; Livnah, N.; Ottolenghi, M. *J. Phys. Chem.* **1996**, *100*, 12066–12075.

(18) Ujj, L.; Volodin, B. L.; Popp, A.; Delaney, J. K.; Atkinson, G. H. *Chem. Phys.* **1994**, *182*, 291–311.

(19) Mathies, R. A.; Lin, S.; Fodor, S. P. A.; Pollard, W. T.; Ames, J.; Gebhard, R.; Vandenberg, E.; Winkel, C.; Lugtenburg, J. *Biophys. J.* **1988**, *53*, A245—A245.

(20) Garavelli, M.; Negri, F.; Olivucci, M. *J. Am. Chem. Soc.* **1999**, *121*, 1023–1029.

(21) Send, R.; Sundholm, D. *J. Phys. Chem. A* **2007**, *111*, 8766–8773.

(22) Vreven, T.; Bernardi, F.; Garavelli, M.; Olivucci, M.; Robb, M. A.; Schlegel, H. B. *J. Am. Chem. Soc.* **1997**, *119*, 12687–12688.

(23) Weingart, O.; Schapiro, I.; Buss, V. *J. Phys. Chem. B* **2007**, *111*, 3782–3788.

(24) Frutos, L. M.; Andruniow, T.; Santoro, F.; Ferre, N.; Olivucci, M. *Proc. Natl. Acad. Sci. U.S.A.* **2007**, *104*, 7764–7769.

(25) Barbatti, M.; Granucci, G.; Persico, M.; Ruckenbauer, M.; Vazdar, M.; Eckert-Maksic, M.; Lischka, H. *J. Photochem. Photobiol. A: Chem.* **2007**, *190*, 228.

(26) Barbatti, M.; Ruckenbauer, M.; Szymczak, J. J.; Aquino, A. J. A.; Lischka, H. *Phys. Chem. Chem. Phys.* **2008**, *10*, 482–494.

(27) Warshel, A. *Nature* **1976**, *260*, 679–683.

(28) Sumita, M.; Saito, K. *Chem. Phys. Lett.* **2006**, *424*, 374–378.

(29) Migani, A.; Robb, M. A.; Olivucci, M. *J. Am. Chem. Soc.* **2003**, *125*, 2804–2808.

(30) Cembran, A.; Bernardi, F.; Olivucci, M.; Garavelli, M. *J. Am. Chem. Soc.* **2004**, *126*, 16018–16037.

(31) Migani, A.; Sinicropi, A.; Ferre, N.; Cembran, A.; Garavelli, M.; Olivucci, M. *Faraday Discuss.* **2004**, *127*, 179–191.

(32) Birge, R. R.; Hubbard, L. M. *Biophys. J.* **1981**, *34*, 517–534.

(33) Weingart, O.; Schapiro, I.; Buss, V. *J. Mol. Model.* **2006**, *12*, 713–721.

(34) Saam, J.; Tajkhorshid, E.; Hayashi, S.; Schulten, K. *Biophys. J.* **2002**, *83*, 3097–3112.

(35) Warshel, A.; Chu, Z. T. *J. Phys. Chem. B* **2001**, *105*, 9857–9871.

(36) Wanko, M.; Hoffmann, M.; Strodet, P.; Koslowski, A.; Thiel, W.; Neese, F.; Frauenheim, T.; Elstner, M. *J. Phys. Chem. B* **2005**, *109*, 3606–3615.

(37) Aquino, A. J. A.; Barbatti, M.; Lischka, H. *ChemPhysChem* **2006**, *7*, 2089–2096.

(38) Burghardt, I.; Cederbaum, L. S.; Hynes, J. T. *Faraday Discuss.* **2004**, *127*, 395–411.

(39) Rohrig, U. F.; Guidoni, L.; Laio, A.; Frank, I.; Rothlisberger, U. *J. Am. Chem. Soc.* **2004**, *126*, 15328–15329.

(40) Rohrig, U. F.; Guidoni, L.; Rothlisberger, U. *ChemPhysChem* **2005**, *6*, 1836–1847.

(41) Sekharan, S.; Sugihara, M.; Buss, V. *Angew. Chem., Int. Ed.* **2007**, *46*, 269–271.

(42) Hoffmann, M.; Wanko, M.; Strodel, P.; Konig, P. H.; Frauenheim, T.; Schulten, K.; Thiel, W.; Tajkhorshid, E.; Elstner, M. *J. Am. Chem. Soc.* **2006**, *128*, 10808–10818.

(43) Hayashi, S.; Tajkhorshid, E.; Schulten, K. *Biophys. J.* **2003**, *85*, 1440–1449.

(44) Wanko, M.; Hoffmann, M.; Strodel, P.; Koslowski, A.; Thiel, W.; Neese, F.; Frauenheim, T.; Elstner, M. *J. Phys. Chem. B* **2005**, *109*, 3606–3615.

(45) Barbatti, M.; Lischka, H. *J. Phys. Chem. A* **2007**, *111*, 2852–2858.

(46) Barbatti, M.; Lischka, H. *J. Am. Chem. Soc.* **2008**, in press, DOI:10.1021/ja800589p.

(47) Migani, A.; Olivucci, M. *Conical Intersections: Electronic Structure, Dynamics & Spectroscopy*; World Scientific Publishing Company: 2004.

(48) Warshel, A.; Barboy, N. *J. Am. Chem. Soc.* **1982**, *104*, 1469–1476.

(49) Liu, R. S. H.; Asato, A. E. *Proc. Natl. Acad. Sci. U.S.A.* **1985**, *82*, 259–263.

(50) Ruiz, D. S.; Cembran, A.; Garavelli, M.; Olivucci, M.; Fuss, W. *Photochem. Photobiol.* **2002**, *76*, 622–633.

(51) Norton, J. E.; Houk, K. N. *Mol. Phys.* **2006**, *104*, 993–1008.

(52) Logunov, I.; Schulten, K. *J. Am. Chem. Soc.* **1996**, *118*, 9727–9735.

(53) Weingart, O.; Buss, V.; Robb, M. A. *Phase Transitions* **2005**, *78*, 17–24.

(54) Garavelli, M.; Celani, P.; Bernardi, F.; Robb, M. A.; Olivucci, M. *J. Am. Chem. Soc.* **1997**, *119*, 6891–6901.

(55) Weingart, O.; Migani, A.; Olivucci, M.; Robb, M. A.; Buss, V.; Hunt, P. *J. Phys. Chem. A* **2004**, *108*, 4685–4693.

(56) Bunge, A. *J. Chem. Phys.* **1970**, *53*, 20–28.

(57) Hehre, W. J.; Ditchfield, R.; Pople, J. A. *J. Chem. Phys.* **1972**, *56*, 2257–2261.

(58) Binkley, J. S.; Pople, J. A.; Hehre, W. J. *J. Am. Chem. Soc.* **1980**, *102*, 939–947.

(59) Tully, J. C. *J. Chem. Phys.* **1990**, *93*, 1061–1071.

(60) Tully, J. C. *Faraday Discuss.* **1998**, *110*, 407–419.

(61) Swope, W. C.; Andersen, H. C.; Berens, P. H.; Wilson, K. R. *J. Chem. Phys.* **1982**, *76*, 637–649.

(62) Butcher, J. *J. Assoc. Comput. Mach.* **1965**, *12*, 124–135.

(63) Granucci, G.; Persico, M. *J. Chem. Phys.* **2007**, *126*, 134114–11.

(64) Hammes-Schiffer, S.; Tully, J. C. *J. Chem. Phys.* **1994**, *101*, 4657–4667.

(65) Lischka, H.; Shepard, R.; Brown, F. B.; Shavitt, I. *Int. J. Quantum Chem.* **1981**, *S.15*, 91–100.

(66) Lischka, H.; Shepard, R.; Pitzer, R. M.; Shavitt, I.; Dallos, M.; Muller, T.; Szalay, P. G.; Seth, M.; Kedziora, G. S.; Yabushita, S.; Zhang, Z. Y. *Phys. Chem. Chem. Phys.* **2001**, *3*, 664–673.

(67) Lischka, H.; Shepard, R.; Shavitt, I.; Pitzer, R. M.; Dallos, M.; Mueller, T.; Szalay, P. G.; Brown, F. B.; Ahlrichs, R.; Boehm, H. J.; Chang, A.; Comeau, D. C.; Gdanitz, R.; Dachsel, H.; Ehrhardt, C.; Ernzerhof, M.; Hoechtl, P.; Irle, S.; Kedziora, G.; Kovar, T.; Parasuk, V.; Pepper, M. J. M.; Scharf, P.; Schiffer, H.; Schindler, M.; Schueler, M.; Seth, M.; Stahlberg, E. A.; Zhao, J.-G.; Yabushita, S.; Zhang, Z.; Barbatti, M.; Matsika, S.; Schuurmann, M.; Yarkony, D. R.; Brozell, S. R.; Beck, E. V.; Blaudeau, J.-P. *COLUMBUS, an ab initio electronic structure program, release 5.9.1*; 2006.www.univie.ac.at/columbus.

(68) Shepard, R.; Lischka, H.; Szalay, P. G.; Kovar, T.; Ernzerhof, M. *J. Chem. Phys.* **1992**, *96*, 2085–2098.

(69) Shepard, R. In *Modern Electronic Structure Theory*; Yarkony, D. R., Ed.; World Scientific: Singapore, 1995; Vol. 1, p 345.

(70) Lischka, H.; Dallos, M.; Shepard, R. *Mol. Phys.* **2002**, *100*, 1647–1658.

(71) Lischka, H.; Dallos, M.; Szalay, P. G.; Yarkony, D. R.; Shepard, R. *J. Chem. Phys.* **2004**, *120*, 7322–7329.

(72) Dallos, M.; Lischka, H.; Shepard, R.; Yarkony, D. R.; Szalay, P. G. *J. Chem. Phys.* **2004**, *120*, 7330–7339.

(73) Barbatti, M.; Granucci, G.; Lischka, H.; Ruckenbauer, M.; Persico, M. *NEWTON-X: a package for Newtonian dynamics close to the crossing seam, version 0.14b*; 2007.. www.univie.ac.at/newtonx.

(74) Worth, G. A.; Hunt, P.; Robb, M. A. *J. Phy. Chem. A* **2003**, *107*, 621–631.

(75) Groenhof, G.; Bouxin-Cademartory, M.; Hess, B.; deVisser, S. P.; Berendsen, H. J. C.; Olivucci, M.; Mark, A. E.; Robb, M. A. *J. Am. Chem. Soc.* **2004**, *126*, 4228–4233.

(76) Groenhof, G.; Schafer, L. V.; Boggio-Pasqua, M.; Goette, M.; Grubmuller, H.; Robb, M. A. *J. Am. Chem. Soc.* **2007**, *129*, 6812–6819.

(77) Fogarasi, G.; Zhou, X. F.; Taylor, P. W.; Pulay, P. *J. Am. Chem. Soc.* **1992**, *114*, 8191–8201.

(78) Vreven, D. L.; Welch, L.; Reichel, F. D. *Invest. Ophthalmol. Visual Sci.* **1997**, *38*, 4221–4221.

(79) González-Luque, R.; Garavelli, M.; Bernardi, F.; Merchán, M.; Robb, M. A.; Olivucci, M. *Proc. Natl. Acad. Sci. U.S.A.* **2000**, *97*, 9379–9384.

(80) Sinicropi, A.; Migani, A.; De Vico, L.; Olivucci, M. *Photochem. Photobiol. Sci.* **2003**, *2*, 1250–1255.

(81) Govindjee, R.; Balashov, S. P.; Ebrey, T. G. *Biophys. J.* **1990**, *58*, 597–608.

(82) Mathies, R. A.; Cruz, C. H. B.; Pollard, W. T.; Shank, C. V. *Science* **1988**, *240*, 777–779.

(83) Kandori, H.; Furutani, Y.; Nishimura, S.; Shichida, Y.; Chosrowjan, H.; Shibata, Y.; Mataga, N. *Chem. Phys. Lett.* **2001**, *334*, 271–276.

CT800148N